ROYAL SOCIETY
OF CHEMISTRY

Convergence of dissolving and melting at the nanoscale†

C. Chen,‡[ad] X. Wang,‡[ae] K. Binder,[b] U. Pöschl, [iD][c] H. Su [iD][c] and Y. Cheng [iD] *[a]

Phase transitions of water and its mixtures are of fundamental importance in physical chemistry, the pharmaceutical industry, materials sciences, and atmospheric sciences. However, current understanding remains elusive to explain relevant observations, especially at the nanoscale. Here, by using molecular dynamics simulations, we investigate the dissolution of sodium chloride (NaCl) nanocrystals with volume-equivalent diameters from 0.51 to 1.75 nm. Our results show that the dissolution of NaCl in aqueous nanodroplets show a strong size dependence, and its solubility can be predicted by the Ostwald–Freundlich equation and Gibbs–Duhem equation after considering a size-dependent solid–liquid surface tension. We find that the structure of dissolved ions in the saturated aqueous nanodropplet resembles the structure of a molten NaCl nanoparticle. With decreasing nanodroplet size, this similarity grows and the average potential energy of NaCl in solution, the molten phase and the crystal phase converges.

Introduction

Water solubility is an important physicochemical property of a substance influencing many processes, such as the absorption of drugs, nucleation in solution and hygroscopic growth of atmospheric nanoparticles.[1–3] Besides chemical composition and temperature, particle size has been recognized as another factor controlling the solubility of nanoparticles.[4–7] For example, size-dependent solubilities have been found for sodium chloride (NaCl) and ammonium sulfate (AS)

[a]*Minerva Research Group, Max Planck Institute for Chemistry, 55122 Mainz, Germany. E-mail: yafang.cheng@mpic.de*

[b]*Institute of Physics, Johannes Gutenberg University of Mainz, Staudinger Weg 7, 55128 Mainz, Germany*

[c]*Multiphase Chemistry Department, Max Planck Institute for Chemistry, Hahn-Meitner-Weg 1, 55128 Mainz, Germany*

[d]*Tsinghua University, 100084 Beijing, China*

[e]*Institute for Carbon-Neutral Technology, Shenzhen Polytechnic, Shenzhen 518055, China*

† Electronic supplementary information (ESI) available. See DOI: **https://doi.org/10.1039/d3fd00095h**

‡ These authors contributed equally to this work.

nanoparticles, which can be well explained by the Ostwald–Freundlich effect.[3] As the particle size of NaCl decreases, increased solubility and dissolution rate have also been reported based on MD simulations.[8,9]

Then comes the question of what will happen if the particle size keeps decreasing, e.g., down to 1 nm or smaller? Will the solubility become infinitely large? What's the state of these nanoparticles? So far, there are very few quantitative studies on size-dependent solubility of nanoparticles with a diameter of 2 nm or smaller. The reason for the few studies is the experimental challenge involved when investigating solubilities of particles of a few nanometers or less.[10–12]

Here, the size-dependent solubility of NaCl nanoparticles in water droplets is investigated for a diameter range from 0.507 to 1.745 nm by classical MD simulations. The size-dependent solid–liquid surface tension and structures under the corresponding critical conditions were also analyzed. In the MD simulations, an improved detection approach is developed to directly distinguish solid-like and liquid-like structures of NaCl nanoparticles in water droplets. With this approach, the solubility of a certain size of NaCl nanoparticles is determined. Then, solid–liquid surface tension and solubility of NaCl nanoparticles at other sizes are calculated by the Gibbs–Duhem equation, the Ostwald–Freundlich equation and the Tolman equation. We also analyzed the structure of saturated aqueous nanodroplets of different sizes. In the end, the connection of dissolution and melting processes and its implications in the phase transition of aerosol particles is also discussed.

Results and discussion

Size-dependent solubility of NaCl nanoparticles

Fig. 1 shows the solubility of NaCl nanoparticles with 7 to 108 pairs of NaCl ions calculated by the MD simulations. Here, we used the q_8 detection method, a local order parameter approach[29] to determine the solubility of NaCl (see Methods section). A strong size dependence of solubility is found for NaCl particles with diameters larger than 0.665 nm (13 pairs of NaCl ions) (red and orange bars in Fig. 1) according to the improved q_8 detection approach. At a particle diameter equal to 0.665 nm with 13 pairs of NaCl ions, the saturation mass fraction is ~3.2 times higher than the simulated saturation mass fraction of bulk NaCl particle (gray circle in Fig. 1).[9,13–16] The trend is qualitatively consistent with the experimental results (green triangles in Fig. 1).[3] The simulated solubility data are a bit lower compared to the experimental data, where the experimental saturation mass fraction of bulk NaCl (brown triangle in Fig. 1) is ~1.5 times higher than the simulated saturation mass fraction of bulk NaCl.

Size-dependent solubility based on the simulations cannot be explained by the combination of the Ostwald–Freundlich and Gibbs–Duhem equations with a single bulk solid–liquid surface tension ($\sigma_{sl,bulk}$) (eqn (3)). The prediction curve obtained based on the single $\sigma_{sl,bulk} = 102$ mN m^{-1} and the bulk saturation mass fraction ($\chi_{s,bulk}^{*}$) calculated by MD simulations[17] (pink line in Fig. 1) does not fit the data well. This indicates that the simulated solubility data become sensitive to σ_{sl} as the crystal gets smaller. Therefore, the size-dependent solid–liquid surface tension of NaCl nanoparticles should be considered to reproduce the size-dependent solubility of NaCl nanoparticles.
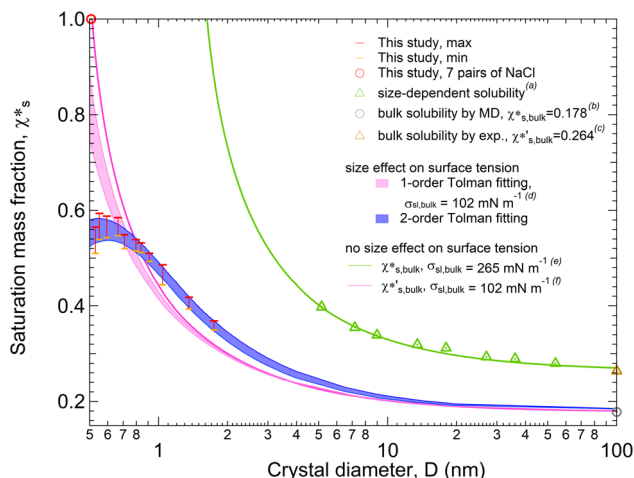
Fig. 1 Size-dependent solubility (saturation mass fraction) of NaCl nanoparticles at 300 K. The solubility range of NaCl nanoparticles is obtained from the MD simulations for particles with 8 to 108 pairs of NaCl ions (red and orange bars) and 7 pairs of NaCl ions (red circle). [a]The size-dependent solubility of NaCl nanoparticles is taken from experiments for particles with dry diameters of 5.18 to 54.2 nm (green triangles). [b,c]The NaCl bulk solubility from MD simulations (grey circle) and from experiment (brown triangle) is taken from ref. 9. The size-dependent solubility curves are obtained based on the combination of the Ostwald–Freundlich and the Gibbs–Duhem equation with and without considering size effects on surface tension. The size effect on solid–liquid surface tension is considered based on the 2nd order Tolman equations for the light blue shaded curves. [d]The size effect on solid–liquid surface tension is considered based on the 1st order Tolman equation with the bulk solid–liquid surface tension from ref. 17 for the light pink shaded curves. [e]The green curve without considering the size effect of surface tension is based on the NaCl bulk solubility obtained experimentally and the bulk solid–liquid surface tension from ref. 3. [f]The pink curve without considering the size effect of surface tension is based on the NaCl bulk solubility from MD simulations and the bulk solid–liquid surface tension from ref. 17.

The saturation mass fraction (χ_s^*) of NaCl particles with diameters less than 0.665 nm does not vary monotonically. The saturation ratio $(\chi_s^*/\chi_{s,bulk}^*)$ remains similar when the diameter of the crystal decreases from 0.665 to 0.530 nm, with 13 to 8 pairs of NaCl ions. The saturation mass fraction suddenly jumps to ~1 when the diameter of the crystal drops to 0.507 nm (7 pairs of NaCl ions), suggesting an infinite solubility. This result is consistent with that in the melting process simulations (Fig. S9†), where the NaCl particle with 7 pairs of NaCl ions is considered as molten at 300 K.

With a size-dependent solid–liquid surface tension (σ_{sl}) based on the second-order Tolman equation (ESI Note 3†),[40–42] the size-dependent solubility from MD simulations can be well explained by the combination of the Ostwald–Freundlich and Gibbs–Duhem equations (blue shaded curves in Fig. 1). Compared to the fitting curves from the first-order Tolman equation (light pink shaded curves in Fig. 1), the blue fitting curves from the second-order Tolman equation better capture the variation of NaCl solubilities. In addition, the size-dependent surface tension competes with the effect of crystal size on the solubility of nanoparticles. The reduction in particle size contributes to an increase in solubility, but this gain

is inhibited by the reduced surface tension, particularly when the particles are smaller than 0.665 nm with 13 pairs of NaCl ions.

Structures of NaCl nanoparticles at different dissolution states

Here, we examined the structures of NaCl nanoparticles at three states of dissolution: the incomplete, critical, and complete dissolutions. By incrementally adding water molecules and the q_8 criteria, we determined the range of water molecule quantities and corresponding solubility range for crystal dissolution. When the number of water molecules surrounding the crystal falls within the solubility range (between the upper and lower limits in Table S1†), we consider it to be in a critical dissolution state. When the crystal is surrounded by fewer water molecules than the solubility range, we consider it to be in an incomplete dissolution state. Conversely, when the crystal is surrounded by more water molecules than the solubility range, we consider it to be in a complete dissolution state. At this stage, we can compare the distribution of NaCl ions and water molecules within the nanoscale particle under the three different states. We find that the distribution of ions and water molecules is inhomogeneous in the incomplete and critical dissolution states, but close to homogeneous in the complete dissolution state. The droplet composed of 32 NaCl pairs (corresponding to 1 nm diameter) with 100 to 160 water molecules is taken as an example, where the particle containing 110–130 water molecules is in the critical dissolution state.

As shown by the light red lines in Fig. 2, in the incomplete dissolution state, both Na^+ and Cl^- ions are primarily distributed within ~1 nm distance from the center of mass (COM) of the particle, and more concentrated within distances of ~0.4 nm. Na^+ ions have the highest density distribution at ~0.3 nm distance from the COM, while Cl^- ions are concentrated at the COM and ~0.4 nm distance from the COM. Meanwhile, water molecules are distributed at distances >0.4 nm and mostly concentrated at distances of ~1 nm from the COM.

As shown by the red and blue lines in Fig. 2, in the critical dissolution state, the concentration distribution of Na^+ and Cl^- ions becomes similar but not homogeneous, and the concentration of ions decreases gradually from the COM to the particle surface. Water molecules are concentrated at a position closer to the COM compared to that in the incomplete dissolution state, and individual water molecules enter the interior of the particle (<0.4 nm distance from the COM). This shows that only a few water molecules are required to destroy the crystal structure inside the NaCl nanoparticle, where saturation can be much higher than that on the surface of the particle.

As shown by the light blue lines in Fig. 2, in the complete dissolution state, the distribution of Na^+ and Cl^- ions is even more similar. This indicates that the distribution of ions and water molecules would be homogeneous when the mass saturation of NaCl particle is close to the bulk mass saturation. Note that the fixed COM position of the total system in the MD algorithm might cause small fluctuations of the nanocrystal position relative to the total COM, which may give rise to some smearing of the profiles of the ion and water molecule densities near the COM of the total system.

The structure of different-size droplets in the critical dissolution state is further analyzed to quantify the characteristics of the inhomogeneous
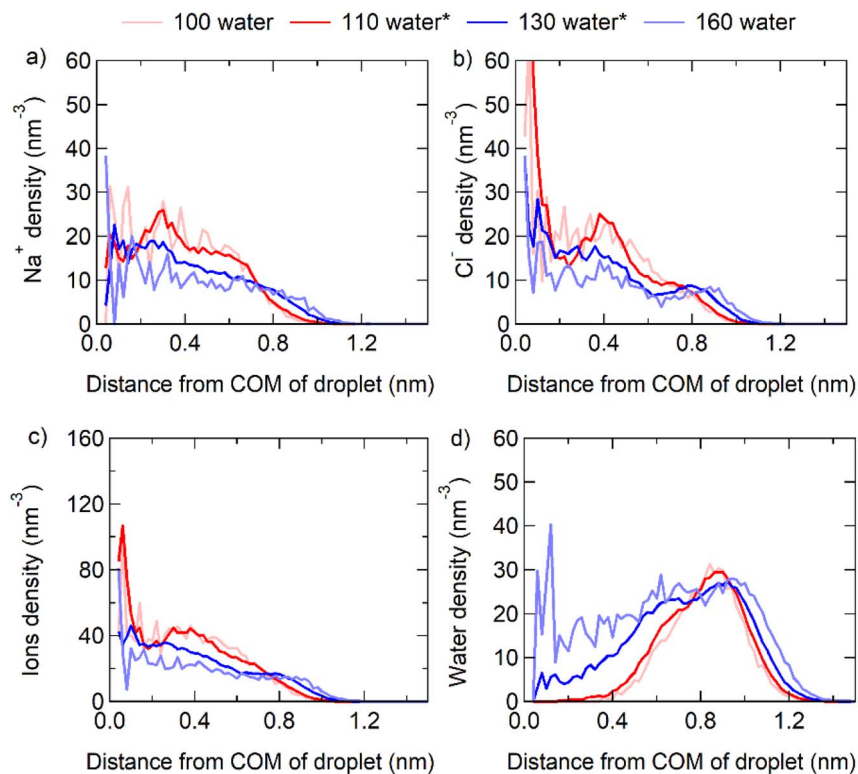
Fig. 2   The number density profiles of ions and water molecules in particles composed of 1 nm NaCl (32 pairs) and different numbers of water molecules for (a) Na^+ ions, (b) Cl^- ions, (c) ions, and (d) water molecules. Particles with less than 110 water molecules are in the incompletely dissolved state (light red lines). Particles with 110–130 water molecules are in the critically dissolved state (red and blue lines), and particles with more than 130 water molecules are saturated NaCl aqueous nanodroplets (light blue lines).

distribution of ions and water. The saturated droplet composed of 32 pairs of NaCl ions (corresponding to 1 nm diameter) with 130 water molecules is taken as an example. As shown in Fig. 3a, the profile of number density of ions and water molecules at different distances from the center of mass (COM) indicates ions are highly concentrated in the area around the COM of the droplet and are more diluted in the area near the surface. For example, the profile of the number of ions and water molecules at different distances from the COM in this droplet suggests only ~4 water molecules exist in the area around the COM of the droplet with a radius of 0.5 nm, while there are 16 ions in the same area (Fig. 3b).

The two-dimensional density map of the relative fraction of ions shows more visually the gradient distribution of the ions (Fig. 3c). Except for a thin interface where no ion exists, the bulk solution with a concentration of 14.4 mol kg^{-1} is homogeneous. This is similar to the result from the previous simulation, where the smooth density profile of ions in the bulk solution with a concentration of 11.48 mol kg^{-1} indicates the homogeneous structure of the system.[18] In contrast, the droplet composed of 32 NaCl and 130 water molecules shows inhomogeneity of the ion/water distribution with a gradient. The concentration becomes larger
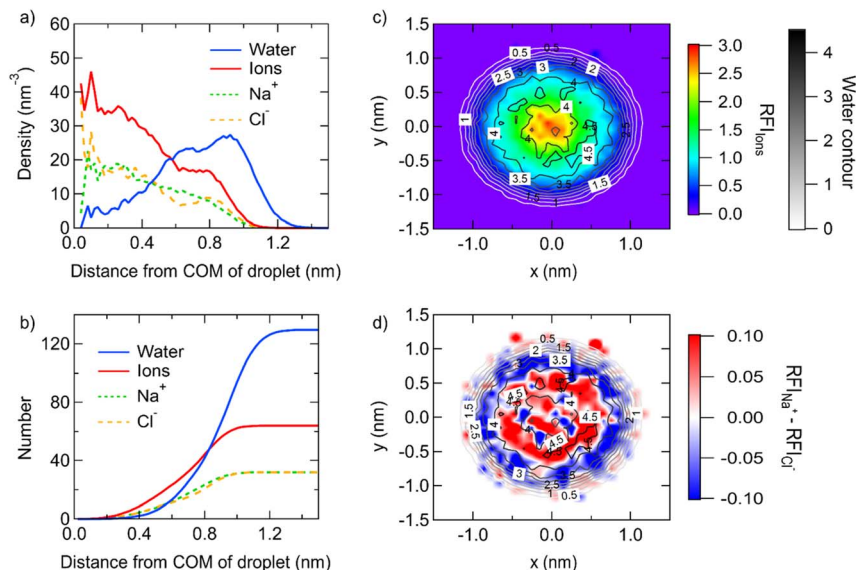
Fig. 3 Distribution of ions and water molecules in the droplet composed of 1 nm NaCl and 130 water molecules. (a) The number density of ions and water molecules at different distances from the COM in the droplet. (b) The cumulative number of ions and water molecules at different distances from the COM in the droplet. (c) Two-dimensional density map of the relative fraction of ions. The contour lines represent the relative fraction of water molecules. (d) Two-dimensional density map of the difference of the relative fraction of Na^+ and Cl^- ions. The contour lines represent the relative fraction of water molecules.

when the position is closer to the center. Furthermore, the distribution of Na^+ and Cl^- ions is rather stratified. The bidimensional density map of the difference of the relative fraction of Na^+ and Cl^- ions (Fig. 3d) shows that Na^+ ions are more concentrated in the center of the droplet, while Cl^- ions are more concentrated at the surface of the droplet.

Dissolution and melting of NaCl nanoparticles

Following the approach of Qi et al.,[19] we determined the melting temperature for the nanocrystals above the size of 15 pairs and the melting points of the NaCl nanocrystals show a clear size dependence (ESI Note 1). As shown in Fig. S8,† the heat capacity (blue circles) is obtained from the derivative of the average potential energy (red circles) with respect to the temperature (see eqn (S1)†), and the melting temperature of each crystal is at the temperature with the maximum apparent heat capacity.

Above the size of 15 pairs of NaCl nanocrystals, the depression of the melting point of the nanocrystals in comparison to the bulk is quite proportional to $N^{(-1/3)}$, showing a significant size dependence (red dashed line in Fig. S9† and N is the number of ions). This phenomenon also occurs in other substances, i.e., pure metal and alloy nanoparticles.[19-21] The dependence can be derived from the decrease in phase stability of the nanoparticles due to surface effects.[22] By using the q_8 calculation, the melting point of the NaCl nanocrystals is also determined

(blue diamonds in Fig. S9†). The results show that above the size of 8 pairs of NaCl nanocrystals, the melting point depression of the nanocrystals is proportional to $N^{(-1/3)}$ (blue dashed line in Fig. S9†). The approach of Qi *et al.*[19] (2001) cannot be applied to determine the melting temperature for NaCl nanocrystals below the size of 15 pairs. Note that the melting temperature for the NaCl nanocrystals below the size of 15 pairs is already less than the Debye temperature, and the heat capacity no longer follows the Dulong–Petit law. The vibrations of the atoms must be considered for accurate heat capacity data.

By comparing the average potential energy of dissolved and molten NaCl nanoparticles with diameters below 6 nm, we find that the structure of dissolved NaCl in saturated solution becomes similar to the structure of molten NaCl when the NaCl particle size decreases. The average potential energy of NaCl (μ_{NaCl}) only depends on the relative position of the ions,[14] so that it can reflect the spatial distribution of the ions. The average potential energies in different simulated systems are compared to analyze the similarity of NaCl in the dissolved state and molten state quantitatively (Fig. 4). Dark circles represent μ_{NaCl} in the molten NaCl particles at the respective melting points, and the values are all close to -700 kJ mol^{-1} (grey line). This means that the spatial distribution of ions in a molten NaCl particle at the respective melting point is almost the same and independent of size. This phenomenon was also found for other substances, such as copper.[23] However, μ_{NaCl} in the dissolved droplets at the critical dissolution state (blue circles) decreases with the decrease of size. The blue circles approach -700 kJ mol^{-1} and deviate from the blue dashed line ($\approx -358.35 \pm 20.95$ kJ mol^{-1}), which represents μ_{NaCl} in bulk saturated solution. It suggests the
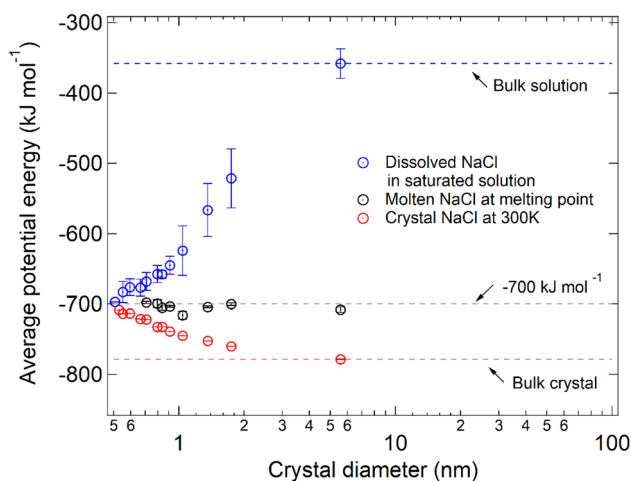

Fig. 4 Average potential energy of NaCl (μ_{NaCl}) in solution, molten NaCl and crystal. Blue circles represent μ_{NaCl} in the saturated droplets at the critical dissolution state. The blue dashed line represents μ_{NaCl} in bulk saturated solution ($\approx -358.35 \pm 20.95$ kJ mol^{-1}). Black circles represent μ_{NaCl} in the molten NaCl at the respective melting points, and the values are all near -700 kJ mol^{-1} (gray dashed line). Red circles represent μ_{NaCl} in the NaCl crystals at 300 K, and the dashed red line is μ_{NaCl} in the bulk NaCl crystal (≈ -780 kJ mol^{-1}).

structural similarity of dissolved NaCl in saturated nanodroplets to molten NaCl at the melting point increases when the size of the NaCl particle decreases.

In Fig. 4, the red circles represent μ_{NaCl} of the NaCl nanoparticles at 300 K, which deviate from the red line that represents μ_{NaCl} of the bulk NaCl crystal (≈ -780 kJ mol^{-1}). The increase of μ_{NaCl} with the decrease of particle size is because the bigger particle is more stable and thus has a higher melting point temperature. As the particle size decreases to ~7 pairs of NaCl ions, the red circles and blue circles almost converge at around -700 kJ mol^{-1}. The convergence of μ_{NaCl} suggests that 7 pairs of NaCl ions at 300 K is in a molten state and can be considered as a saturated droplet of NaCl with infinite solubility. Due to the size-dependent solubility, smaller molten NaCl particles at 300 K (≤ 7 pairs of NaCl ions) can also be considered as a saturated droplet of NaCl with infinite solubility.

The radius of gyration of the particles and the radial distribution function of ions to ions (RDF$_{ion-ion}$) also supports the analysis of μ_{NaCl}. The similarity of the radius of gyration of the NaCl particles in the dissolution and melting processes becomes more pronounced when the particle size decreases (Fig. 5). The similarity of the relative positions of ions in the dissolution and melting processes increases when the particle size decreases (Fig. S12†). Harbury[4] gave a similar assumption that there is a significant comparability between a supersaturated
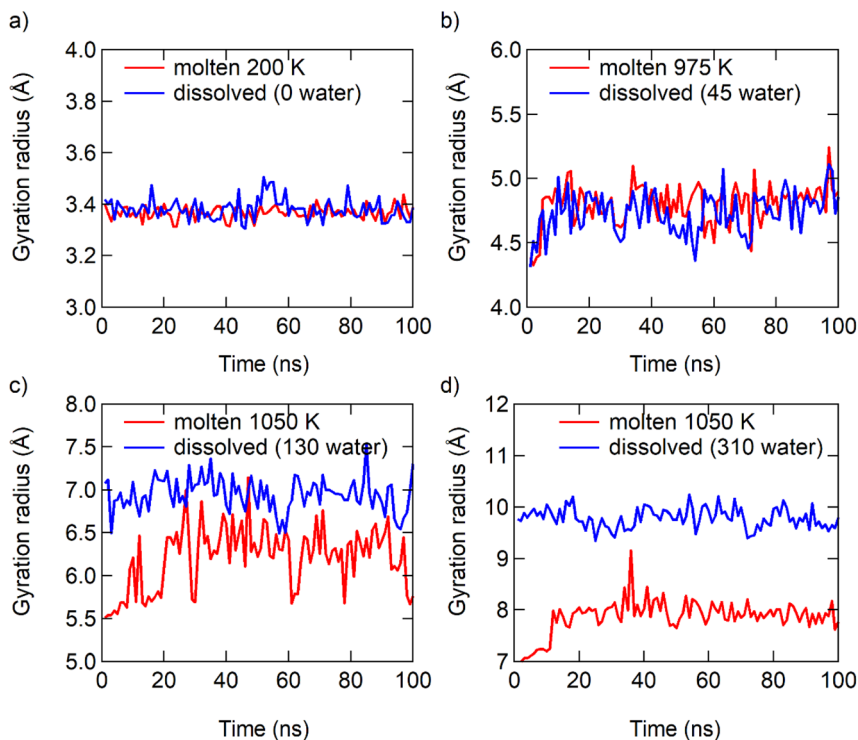

Fig. 5 The radius of gyration of the molten NaCl and dissolved NaCl in saturated solution nanodroplets for (a) 7 pairs of NaCl ion particles (diameter = 0.507 nm), (b) 15 pairs of NaCl ion particles (diameter = 0.709 nm), (c) 32 pairs of NaCl ion particles (diameter = 1.042 nm) and (d) 62 pairs of NaCl ion particles (diameter = 1.358 nm).

solution and undercooled melts. In summary, the dissolution of bulk NaCl solids is a traditional dissolution, while the dissolution of NaCl particles at the nano-scale is analogous to the melting process of NaCl particles at the nanoscale. These two different types of phase transition, dissolving and melting, "meet" at ≤7 pairs of NaCl ions at 300 K.

The radial distribution functions of Na^+ to Na^+ (RDF_{Na-Na}), Cl^- to Cl^- (RDF_{Cl-Cl}), Na^+ to Cl^- (RDF_{Na-Cl}), and Cl^- to Na^+ (RDF_{Cl-Na}) give valuable additional information that the q_8-determined solubility and melting point of NaCl nano-crystals are on firm ground. The RDF_{Na-Na} and RDF_{Cl-Cl} of the q_8-determined unmelted NaCl nanocrystals and undissolved NaCl in saturated nanodroplets show rather sharp peaks at the first to fourth nearest neighbor distances of ∼0.40 nm, ∼0.56 nm, ∼0.69 nm, and ∼0.79 nm (Fig. S13 and S15†). The RDF_{Na-Cl} and RDF_{Cl-Na} of the q_8-determined unmelted NaCl nanocrystals and undissolved NaCl in saturated nanodroplets show the same sharp peaks at the first to fourth nearest neighbor distances of ∼0.28 nm, ∼0.49 nm, ∼0.63 nm, and ∼0.84 nm (Fig. S17 and S19†). This is well compatible with the simple predictions from the snapshot of 9 pairs in a NaCl crystal shown in Fig. S20,† indicating that the nanocrystals are still crystalline despite their smallness, and the crystal structure is not disturbed by the condensation of a few water molecules. Meanwhile, the RDF_{Na-Na} and RDF_{Cl-Cl} as well as the RDF_{Na-Cl} and RDF_{Cl-Na} of the q_8-determined molten NaCl nanocrystals at the melting points and dissolved NaCl in saturated nanodroplets show flatter peaks compared to the ones of the unmelted and undissolved NaCl nanoparticles (Fig. S12, S14, S16 and S18†). This captures well the different structural features between the solid and liquid states of NaCl, thus supporting the results of the solubility and melting point of NaCl nanoparticles determined by the q_8 method. Snapshots of NaCl nanoparticles during the melting and dissolution processes in Fig. S20† support the solubility and melting point of NaCl nanoparticles determined by the q_8 method as well. The snapshots of NaCl nanoparticles at a temperature lower than the q_8-determined melting points show that the typical shape of nano-sized NaCl nanocrystals is not spherical. Both in the case of melting and the dissolution process, a spherical shape occurs only when the transition to the fluid phase takes place.

Implications

Our MD simulations demonstrate that the solubility of NaCl at the nanoscale is size-dependent and can be much higher than that of a bulk solution. The melting point of NaCl is also found to be size-dependent. To transform a NaCl particle with a temperature of 300 K into the liquid state, the temperature of the envi-ronment should be increased or water should be added to the NaCl. In these processes, heat from a higher-temperature environment or the interaction with water molecules changes the NaCl crystal to the liquid state. In other words, the heat, and the interaction with water for NaCl nanocrystals are equivalent. As the size decreases, a lower temperature or less surrounding water molecules are needed to change the phase of NaCl. The nanoparticle with only 7 pairs of NaCl ions cannot exist in the solid state at 300 K, thus no heat or interaction with a few water molecules is needed to transform it into liquid.

Overall, this study provides a new perspective to connect the dissolution and melting processes of NaCl nanoparticles, and this connection may also be

suitable for other solids. For a substance whose melting point is higher than 300 K at the macroscopic level, there exists a critical diameter (D_c) at which the melting point is 300 K. Naturally, when the diameter of the nanoparticle composed by this substance is below D_c, the particle is expected to be liquid at room temperature. The nanoparticle whose diameter is larger than D_c is solid at room temperature, while a small amount of adsorbed water molecules can turn it into a molten-like liquid with a thin solution coating. These general principles may be useful for studies about nanoparticles in various fields, including the environmental, pharmaceutical and materials sciences.[24–26] This study mainly focuses on the thermodynamics of dissolution. A deep understanding of the NaCl dissolution mechanism also requires knowledge of the kinetics, and we would like to direct the readers to other related research.[27,28]

Methods

MD simulations

The Joung–Cheatham (JC) force field for NaCl with the SPC/E water model has been proved to nicely predict the experimental value of solubility (∼6.15 mol kg^{-1}).[9,13–16] Therefore, this force field combination is applied in the study to simulate the NaCl–water mixture. The MD simulations are carried out with the GROMACS 2016.6 package.[29,30] NaCl nanocrystals with different diameters are surrounded by certain water molecules initially. The systems are then energetically minimized by the steepest-descent method and equilibrated for 100 ps at 300 K. The MD simulations are further performed in the NVT ensemble with periodic boundary conditions and velocity-rescaling thermostat. Electrostatic interactions are calculated using the particle mesh Ewald (PME) algorithm, and van der Waals interactions are accounted for up to a cutoff distance of 10 Å. All simulations are carried out for at least 600 ns using a 1 fs time step, and conformations for analysis are saved every 2 ps. To determine the solubility, we kept increasing the number of water molecules in the system until we found a critical number that allows NaCl to dissolve completely based on the q_8 algorithm. Ideally, we would add water molecules one by one, but in practice, due to the limitations of the computational resources, we increased the step size by 5 to 20 molecules. Thus, instead of an exact number, we determine a narrow range of water molecules required for crystal dissolution and Table S1† summarizes the upper and lower limits of this range. We chose a simulation duration of at least 600 ns, ensuring that even the largest simulated NaCl nanoparticle (108 pairs of NaCl ions with 650 water molecules, ∼1.745 nm diameter) would completely dissolve (Fig. S10†). Each simulation box has a uniform size of 10 × 10 × 10 nm^3, ensuring it can accommodate the largest simulated NaCl nanoparticle (108 pairs of NaCl ions with 650 water molecules, ∼1.745 nm diameter). More detailed information about the number of ions/water molecules, the initial structure setup, and simulation times are summarized in Table S1 and Fig. S11.†

In this study, the melting processes of NaCl nanocrystals is also simulated. The JC force field is adopted to keep synchronous with the simulations of the NaCl dissolution process. The particles with different diameters are simulated at different temperatures to determine the melting point. More details about the setup are shown in ESI Note 1.†

Solubility determination: q_8 detection approach

To detect the dissolution and melting progress of NaCl nanocrystals, it is important to distinguish ions that are in the solid-like and liquid-like structures. To do this, the local order parameter approach of Steinhardt $et\ al.$[31] is adopted. For each ion (i), the local bond-orientational order parameter $q_l(i)$ is calculated as:

$$q_l(i) = \left[\frac{4\pi}{2l+1} \sum_{m=-l}^{l} |q_{lm}(i)|^2 \right]^{\frac{1}{2}} \tag{1}$$

and

$$q_{lm}(i) = \frac{1}{N} \sum_{j=0}^{N} Y_l^m \left(\theta(r_{ij}), \varnothing(r_{ij}) \right), \tag{2}$$

where l is a free integer parameter and m is an integer that runs from $m = -l$ to l. Y_l^m is the spherical harmonic, r_{ij} is the position vector of the neighbor ion (j) with respect to the central ion (i), $\theta(r_{ij})$ and $\varnothing(r_{ij})$ are the polar and azimuthal angles with respect to the reference coordinate of r_{ij}. N is the number of neighboring ions. Note that in the perfect bulk NaCl crystal structure, each ion has 6 nearest neighbors of different species ($e.g.$, Na^+ has 6 neighboring Cl^- ions and $vice\ versa$) and 12 next-nearest neighbors of the same kind ($e.g.$, Na^+ has 12 neighboring Na^+ ions). However, the NaCl nanoparticle structures during the melting and dissolution processes in the simulations are mostly not perfect crystal structures. Therefore, here the ions are considered to be identical and the number of neighboring ions is equal to 12. Lanaro and Patey[32] utilized a similar method to track the production of NaCl nuclei in aqueous solutions. Jiang $et\ al.$[33] also used this approach to investigate the mechanism of NaCl crystal nucleation from solutions with high supersaturations. The parameter $q_l(i)$ is sensitive to different crystal symmetries depending on the choice of l. $q_l(i)$ distributions for $l = 4$, 6, and 8 were examined, using the cubic nanocrystal with 108 pairs of NaCl in the solid phase and the dissolved state as representative of the liquid phase at 300 K. As shown in Fig. S3,† the local bond-orientational order parameter $q_8(i)$ provides the best separation between solid and liquid phase distribution for NaCl nanoparticles.

The NaCl nanocrystal is considered as dissolved or molten when the time average of the q_8 value of each ion in the crystal is less than 0.35. q_8 is the local bond-orientational order parameter to provide the best separation between solid-like (>0.35) and liquid-like (≤0.35) states of each NaCl ion in the nanoparticles (Fig. S5†). We added 5 water molecules each time for the certain NaCl nanocrystal in the simulation. The crystal with $N + 5$ water molecules is considered as dissolved when the time average of the q_8 value of each ion in the crystal is less than 0.35. At this point, we consider the solubility range of the crystal to be within the range of water molecule quantities of N to $N + 5$. Furthermore, based on the known molar masses of NaCl ions and water molecules, we can calculate the corresponding range of saturated mass fraction values, which represents the solubility range.

Since at 300 K the crystal structure of NaCl is already close to perfectly rigid, a simple study of the radial pair distribution functions between the different pairs

of ions can clearly identify which NaCl clusters are still in a nanocrystal state and which are already in a liquid state (Fig. S6†).

Size-dependent solubility estimation

Size-dependent solubility can be determined by the combination of the Ostwald–Freundlich[6,7] and Gibbs–Duhem equations[34–36] as:

$$RT \int_{x^*_{s,\text{bulk}}}^{x^*_s} M \frac{1 - x_s}{x_s} \, \mathrm{d} \ln a_w = -\frac{4\nu\sigma_{sl}}{D}, \tag{3}$$

where R is the universal gas constant, T is the temperature, ν is the molar volume of solid phase NaCl (atomic volume) given as 2.7×10^{-5} m^3 mol^{-1}, and M is the molar weight of solute. $x^*_{s,\text{bulk}}$ is the mass fraction of solute in a saturated bulk solution, and $a^*_{s,\text{bulk}}$ is the solute activity at $x^*_{s,\text{bulk}}$. x^*_s is the mass fraction of solute in a saturated droplet of diameter D. a_w is the water activity retrieved from the modified Tang–Munkelwitz (TM) model (ESI Note 2†).[3,38] σ_{sl} is the size-dependent solid–liquid surface tension estimated by the Tolman equation (ESI Note 3†).[39] In this study, D is the volume equivalent diameter of a NaCl crystal at the saturation dissolution point, which is equal to the diameter of the NaCl droplet of equivalent volume,

$$D = \sqrt[3]{\frac{6V}{\pi}}, \tag{4}$$

and the volume of the NaCl crystal (V) is measured based on the initial structure in the MD simulations, where the distance between Na$^+$ and Cl$^-$ is 0.28 nm.

Structure analysis

The profiles of number density and number of ions and water molecules at different distances from the center of mass (COM) are used to analyze the structure of saturated droplets. The relative fraction of ions is calculated by the following equation:

$$\mathrm{RFI} = \frac{\rho_{\text{ion.area}}/\rho_{\text{water.area}}}{\rho_{\text{ion.total}}/\rho_{\text{water.total}}} \tag{5}$$

where $\rho_{\text{ion.area}}$ represents the number density of NaCl in a spherical shell area, $\rho_{\text{water.area}}$ represents the number density of water in a spherical shell area, the thickness of the spherical shell is 0.02 nm. $\rho_{\text{ion.total}}$ represents the number density of NaCl in the entire droplet, $\rho_{\text{water.total}}$ represents the number density of water in the entire droplet.

The radial distribution functions (RDFs) of ions with respect to other ions can reflect the spatial distribution of ions.[29,37] They are calculated as:

$$G_{\text{ion–ion}}(r, t_o) = \frac{1}{500} \cdot \sum_{t=0.002}^{1} g_{\text{ion–ion}}(r, t_o + t) \tag{6}$$

Here, $g_{\text{ion–ion}}(r)$ represents the RDF for one conformation:

$$g_{\text{ion–ion}}(r) = \frac{1}{N_{\text{ion}}} \cdot \sum_{i \in N_{\text{ion}}}^{N_{\text{ion}}} \sum_{j \in N_{\text{ion}}}^{N_{\text{ion}}} n(r_{ij}) \tag{7}$$

r represents a given distance and the interval value is the thickness of a spherical shell equal to 0.02 nm, N_{ion} represents the number of ions for the given conformation, i and j represent the ions and $i \neq j$, r_{ij} represents the distance from ions i and ions j, $n(r_{ij})$ represents the number of ions j locates in the distance of $r - 0.02$ nm to r from the given reference ion i. $g_{ion–ion}(r,t_o)$ represents the average value of RDF from t_o to $t_o + 1$ ns. As the simulation time step is 0.002 ns, $g_{ion–ion}(r,t_o)$ can be considered as the average value of 500 conformations, $g_{ion–ion}(r,t_o + t)$ is the RDF at the time $t_o + t$. In this study, RDF$_{ion–ion}$ represents $g_{ion–ion}(r,t_o)$. The profile of RDF$_{ion–ion}$ over time can reflect the change of relative positions of ions during the process of dissolving.

Average potential energy calculation

To calculate the average potential energy of dissolved or molten NaCl, the trajectories only containing the Na$^+$ and Cl$^-$ ions after the MD simulations of a given NaCl–water system are extracted and then rerun for the new trajectories. In the rerun simulation, energy is calculated every 2 ps, and the average value over the time after the equilibrium of a system is taken to describe the system.

Radius of gyration

The radius of gyration is defined as:

$$R_g{}^2 = \frac{1}{N}\sum_i (R_i - R_{COM})^2, \qquad (8)$$

where N is the number of ions in the cluster, R_i is the position of ion (i) and R_{COM} is the position of the center of mass of the cluster.

Conflicts of interest

Authors declare that they have no competing interests.

Acknowledgements

Notes and references

1 R. H. Müller, C. Jacobs and O. Kayser, *Adv. Drug Delivery Rev.*, 2001, **47**, 3–19.
2 N. T. Thanh, N. Maclean and S. Mahiddine, *Chem. Rev.*, 2014, **114**, 7610–7630.
3 Y. Cheng, H. Su, T. Koop, E. Mikhailov and U. Poschl, *Nat. Commun.*, 2015, **6**, 5923.
4 L. Harbury, *J. Phys. Chem.*, 1946, **50**, 190–199.
5 R. H. Müller and K. Peters, *Int. J. Pharm.*, 1998, **160**, 229–237.
6 W. Ostwald, *Z. Phys. Chem.*, 1900, **34U**, 495–503.
7 H. Freundlich, *Kapillarchemie, eine Darstellung der Chemie der Kolloide und verwandter Gebiete*, akademische Verlagsgesellschaft, 1922.
8 G. Lanaro and G. N. Patey, *J. Phys. Chem. B*, 2015, **119**, 4275–4283.

9 J. R. Espinosa, J. M. Young, H. Jiang, D. Gupta, C. Vega, E. Sanz, P. G. Debenedetti and A. Z. Panagiotopoulos, *J. Chem. Phys.*, 2016, **145**, 154111.

10 I. Tang, H. Munkelwitz and N. Wang, *J. Colloid Interface Sci.*, 1986, **114**, 409–415.

11 C. K. Chan, Z. Liang, J. Zheng, S. L. Clegg and P. Brimblecombe, *Aerosol Sci. Technol.*, 1997, **27**, 324–344.

12 C. Vicente, W. Yao, H. Maris and G. Seidel, *Phys. Rev. B*, 2002, **66**, 214504.

13 H. Berendsen, J. Grigera and T. Straatsma, *J. Phys. Chem.*, 1987, **91**, 6269–6271.

14 I. S. Joung and T. E. Cheatham III, *J. Phys. Chem. B*, 2008, **112**, 9020–9041.

15 J. L. Aragones, E. Sanz and C. Vega, *J. Chem. Phys.*, 2012, **136**, 244508.

16 F. Moučka, I. Nezbeda and W. R. Smith, *J. Chem. Phys.*, 2013, **138**, 154102.

17 R. Bahadur and L. M. Russell, *Aerosol Sci. Technol.*, 2008, **42**, 369–376.

18 X. Wang, C. Chen, K. Binder, U. Kuhn, U. Pöschl, H. Su and Y. Cheng, *Atmos. Chem. Phys.*, 2018, **18**, 17077–17086.

19 Y. Qi, T. Çağin, W. L. Johnson and W. A. Goddard III, *J. Chem. Phys.*, 2001, **115**, 385–394.

20 P. Couchman and W. Jesser, *Nature*, 1977, **269**, 481–483.

21 C. Chen, J.-G. Lee, K. Arakawa and H. Mori, *Appl. Phys. Lett.*, 2011, **99**, 013108.

22 Q. Jiang and C. Yang, *Curr. Nanosci.*, 2008, **4**, 179–200.

23 F. Delogu, *Phys. Rev. B: Condens. Matter Mater. Phys.*, 2005, **72**(20), 205418.

24 B. E. Rabinow, *Nat. Rev. Drug Discovery*, 2004, **3**, 785–796.

25 T. Koop, J. Bookhold, M. Shiraiwa and U. Pöschl, *Phys. Chem. Chem. Phys.*, 2011, **13**, 19238–19255.

26 L. Suo, Y.-S. Hu, H. Li, M. Armand and L. Chen, *Nat. Commun.*, 2013, **4**, 1481.

27 J. Klimeš, D. R. Bowler and A. Michaelides, *J. Chem. Phys.*, 2013, **139**, 234702.

28 L. M. Liu, A. Laio and A. Michaelides, *Phys. Chem. Chem. Phys.*, 2011, **13**, 13162–13166.

29 D. Van Der Spoel, E. Lindahl, B. Hess, G. Groenhof, A. E. Mark and H. J. Berendsen, *J. Comput. Chem.*, 2005, **26**, 1701–1718.

30 M. J. Abraham, T. Murtola, R. Schulz, S. Páll, J. C. Smith, B. Hess and E. Lindahl, *SoftwareX*, 2015, **1–2**, 19–25.

31 P. J. Steinhardt, D. R. Nelson and M. Ronchetti, *Phys. Rev. B*, 1983, **28**, 784–805.

32 G. Lanaro and G. N. Patey, *J. Phys. Chem. B*, 2016, **120**, 9076–9087.

33 H. Jiang, P. G. Debenedetti and A. Z. Panagiotopoulos, *J. Chem. Phys.*, 2019, **150**, 124502.

34 M. D. Cohen, R. C. Flagan and J. H. Seinfeld, *J. Phys. Chem.*, 1987, **91**, 4583–4590.

35 C. Richardson and T. D. Snyder, *Langmuir*, 1994, **10**, 2462–2465.

36 J. H. Seinfeld, S. N. Pandis and K. Noone, *Phys. Today*, 1998, **51**, 88.

37 B. Hess, L. E. van der Spoel and E. Lindahl, *User Manual*, Version 4, 2010.

38 I. N. Tang, *J. Geophys. Res.: Atmos.*, 1996, **101**, 19245–19250.

39 R. C. Tolman, *J. Chem. Phys.*, 1949, **17**, 333–337.

40 D. Erdemir, A. Y. Lee and A. S. Myerson, *Acc. Chem. Res.*, 2009, **42**, 621–629.

41 N. E. Zimmermann, B. Vorselaars, D. Quigley and B. Peters, *J. Am. Chem. Soc.*, 2015, **137**, 13352–13361.

42 B. Patrov, *Zh. Prikl. Khim.*, 1997, **70**, 1900–1902.